184, 263 (1969).
[23]C. P. Bean and D. S. Rodbell, Phys. Rev. 126, 104 (1962).
[24]E. V. Baklanov and A. V. Chaplik, Fiz. Tverd. Tela 7, 2768 (1965)[Soviet Phys. Solid State 8, 175 (1966)].

PHYSICAL REVIEW B VOLUME 2, NUMBER 9 1 NOVEMBER 1970

Study of the Spin-Reordering Transition in Cr_5S_6 †

K. Dwight, N. Menyuk, and J. A. Kafalas
Lincoln Laboratory, Massachusetts Institute of Technology, Lexington, Massachusetts 02173
(Received 16 June 1970)

It is known that Cr_5S_6 becomes ferrimagnetic at $T_C = 305\,°K$ and undergoes a ferrimagnetic-antiferromagnetic transition at $150 < T_t < 160\,°K$. A neutron-diffraction study by van Laar indicates this transition to be of second order, whereas the existence of thermal hysteresis points to a first-order effect. We have investigated the magnetization of Cr_5S_6 as a function of hydrostatic pressure as well as of temperature and applied field. We find that $\partial T_C/\partial P = 1.83\,°K/kbar$, $\partial T_t/\partial P = 0.04\,°K/kbar$, and $\sigma_0^{-1}(\partial\sigma_0/\partial P) = -0.011/kbar$. $\partial T_t/\partial H$ runs from $-0.54\,°K/kOe$ at low fields to $-0.45\,°K/kOe$ at 9–12 kOe; these values, together with the shape of the normalized curve of magnetization versus temperature, are independent of pressure. In addition, we have investigated theoretically the classical ground-state spin configuration of the Cr_5S_6 lattice, using the generalized Luttinger-Tisza method, and have computed the thermal evolution of the ground state in the molecular field approximation. The observed spiral ground state is found to require not only that all the nearest-neighbor interactions be antiferromagnetic, but also that antiferromagnetic next-nearest-neighbor interactions be present. The calculated temperature dependencies of spins on the different sublattices lead directly to a second-order spin transition to a collinear ferrimagnetic configuration at T_t, in good agreement with experiment. We conclude that the transition at T_t is basically of second order, with secondary magnetostrictive forces responsible for the thermal hysteresis. The pressure dependence of σ_0 indicates that some of the magnetization of Cr_5S_6 arises from band electrons. The decrease of T_C with pressure is largely due to a decrease in the nearest-neighbor interaction along the c axis, which interaction is also the one most likely to involve band electrons.

I. INTRODUCTION

The structure of Cr_5S_6 has been determined as similar to that of NiAs, but with ordered vacancies.[1] The material is metallic,[2] has a ferrimagnetic Curie point of 305 °K, and undergoes a ferri-antiferromagnetic transition at 150–160 °K.[3–5] A recent neutron-diffraction study of Cr_5S_6 by van Laar[6] has shown the spin configuration to change from collinear Néel-type ferrimagnetism above the transition temperature (T_t) to a spiral configuration below T_t. van Laar also observed that the wave vector $\vec{k}$ which characterizes the spiral configuration varies in a smooth and continuous fashion from temperatures well below the transition to zero wavelength at and above T_t. This result indicates that the transition between the two magnetic states is of second order, but is at variance with the significant hysteresis observed for T_t, depending on whether the transition is observed during a heating or cooling cycle, which indicates a first-order transition.

In order to gain greater insight into the magnetic behavior of Cr_5S_6 we have undertaken a further study of its magnetic properties as functions of pressure as well as of magnetic field and temperature. We have also applied the generalized Luttinger-Tisza method[7] to study the ground-state configuration of Cr_5S_6 in a multidimensional magnetic-interaction parameter space. This has enabled us to establish the existence of a region in the space wherein the ground-state configurations are of the type observed by neutron diffraction. The variation with temperature of the configurations within this region was then studied in the molecular field approximation.

The effects of pressure on a sample of the slightly different material $CrS_{1.17}$ have been studied previously by Kamigaichi *et al.*[8] They noted kinks in the electrical conductivity at both T_t and T_C, and measured the changes in the temperatures of these kinks as functions of pressure. Since the measurements were of electrical conductivity, they could provide no insight to possible changes of a magnetic character. It also seemed preferable to choose a sample composition which more closely approximated the pure ferrimagnetic phase Cr_5S_6. As will be noted in Sec. II, our results at the transition temperature significantly differ from the results of Kamigaichi *et al.*[8]

II. EXPERIMENTAL RESULTS

Our measurements were made on a sample of

$CrS_{1.194}$. The method of preparation and analysis of the sample have been described previously.[5] All the magnetic measurements were performed using a vibrating-coil magnetometer (VCM). Since the sample is physically isolated in the VCM, the magnetometer can be used with a suitable high-pressure system to obtain measurements of the magnetic moment throughout a large region of the magnetic field-temperature-pressure phase space.[9] Within this region of phase space, H, P, and T can be freely and independently varied.

Initial measurements of the magnetic moment at atmospheric pressure in the vicinity of the transition temperature indicated a rather broad transition as well as a significant amount of hysteresis. In addition, the shape of the transition curve during the cooling cycle broadened significantly upon increasing the applied magnetic field. This change in shape could render meaningless any comparison between cooling-curve transition temperatures obtained in different applied fields. On the other hand, the warming curves have a maximum slope $(\Delta\sigma/\Delta T)_{max}$ which is essentially independent of the applied field, and hence is suitable for defining T_t. However, it should be noted that this transition, though fairly sharp, is not abrupt, with most of the transition occurring over a 4-deg temperature interval. In our measurements, T_t is defined as the temperature on the warming curve at which the magnetic moment of the sample is midway between its maximum value and the value at the intersection of the extension of $(\Delta\sigma/\Delta T)_{max}$ with that of the magnetic moment curve obtained at temperatures below the transition.

The variation of T_t with applied fields up to 12 kOe was investigated both at atmospheric pressure and at 5 kbar. Except for the slight shift in absolute temperature values, as noted below, the behavior was the same in both cases within experimental accuracy. At both low (0–6 kOe) and high (9–12 kOe) magnetic fields, the variation of T_t with field was essentially constant with values of $(\Delta T_t/\Delta H)_P$ of -0.54 and -0.45 deg/kOe, respectively, with a smoothly curving, nonlinear relationship at the intermediate fields. The value obtained at the higher fields is in reasonable accord with the value -0.437 deg/kOe obtained at high pulsed fields by Flippen and Darnell[10] in $CrS_{1.17}$.

The effects of pressure on both the Curie point T_C and the transition temperature T_t were determined and are shown in Fig. 1. In both cases the temperature variation with pressure was linear with $\partial T_C/\partial P = -1.83$ deg/kbar and $\partial T_t/\partial P = 0.04 \pm 0.01$ deg/kOe. The Curie temperature variation is somewhat smaller than the value -2.6 deg/kOe obtained from electrical conductivity measurements on $CrS_{1.17}$ by Kamigaichi *et al*,[8] and our result is very different from their value of $\partial T_t/\partial P = 3.5$ deg/kOe.

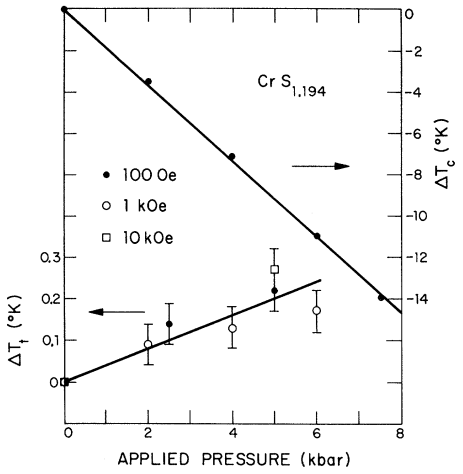

FIG. 1. Variation of T_C and T_t with pressure, showing that the changes in T_t are independent of applied magnetic field within experimental error.

This difference cannot be attributed solely to the difference in sample compositions.[11]

In addition to its effect on the transition and Curie temperatures, pressure was also found to depress the net magnetic moment of our sample throughout the ferrimagnetic range. For example, the application of 5 kbar reduces the maximum moment attainable in 8 kOe (σ_{max}) from 6.42 to 6.05 emu/g. The observed change in magnetic moment can be due either to the effect of pressure on the Curie temperature, or to its effect on the intrinsic moment of the ions, or to both. The relative contribution of these terms to the over-all change is determined by the thermodynamic relationship[12]

$$\frac{1}{\sigma}\left(\frac{\partial\sigma}{\partial P}\right)_{H,T} = \left[\frac{1}{\sigma_0}\left(\frac{\partial\sigma_0}{\partial P}\right)_{H,T} - \frac{1}{\sigma}\left(\frac{\partial\sigma}{\partial T}\right)_{P,H}\frac{T}{T_C}\left(\frac{\partial T_C}{\partial P}\right)\right] \div \left[1+\frac{3\alpha}{\kappa}\,\frac{T}{T_C}\left(\frac{\partial T_C}{\partial P}\right)\right], \quad (1)$$

where σ is the saturation moment at temperature T, σ_0 is the saturation moment at 0 °K, α is the coefficient of thermal expansion, and κ is the compressibility. At 195 °K, $T/T_C = 0.636 (P=0)$, $(1/\sigma)(\partial\sigma/\partial P) = -0.017$/kbar, and $(1/\sigma)(\partial\sigma/\partial T) = -0.00506$/°K. Substituting these results, along with the previously obtained value $(\partial T_C/\partial P) = -1.83$ deg/kbar, into Eq. (1) yields

$$-0.017 = \left[\frac{1}{\sigma_0}\left(\frac{\partial\sigma_0}{\partial P}\right)_{H,T} - 0.0059\right] \Big/ \left[1-\frac{3.49\alpha}{\kappa}\right] \quad (2)$$

or

$$\frac{1}{\sigma_0}\left(\frac{\partial\sigma_0}{\partial P}\right)_{H,T} = -0.011 + \frac{0.059\alpha}{\kappa}.$$

The thermal expansion coefficient α for $CrS_{1.17}$

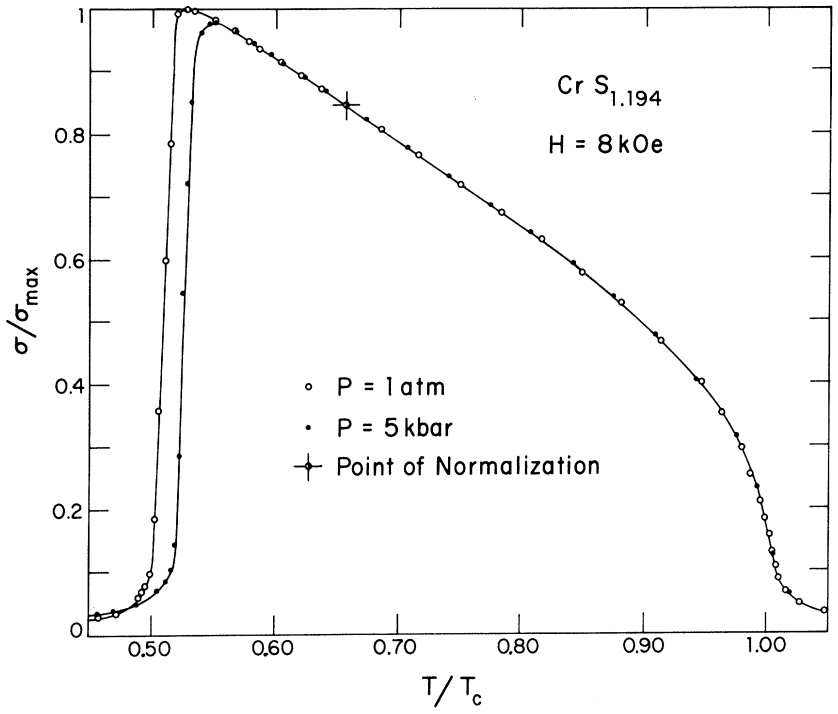

FIG. 2. Normalized magnetization curves obtained in 8 kOe at 5 kbar and at atmospheric pressure. In addition to the temperature normalization, the magnetization values have been normalized at the indicated point.

is approximately[4] $2\times 10^{-5}/^{\circ}\mathrm{K}$, and while κ is unknown, $1\text{-}2\times 10^{-3}$/kbar is a reasonable limiting set of probable values. For these values, the last term in Eq. (2) can be ignored and we are left with the conclusion that, if Eq. (1) is valid for Cr_5S_6, approximately two-thirds of the observed change in moment σ with pressure is due to a change in σ_0.

Equation (1) is normally applied to a ferromagnet, and assumes that

$$\sigma/\sigma_0 = f(T/T_C), \tag{3}$$

where the form of the function $f(T/T_C)$ is independent of pressure. To test the validity of Eq. (3) for Cr_5S_6, the magnetization-versus-temperature curves in 8 kOe at 1 atm and at 5 kbar were redrawn as normalized curves. The Curie point shift at 5 kbar was taken as $P(\partial T_C/\partial P) = -9.15\ ^{\circ}\mathrm{K}$, while the relative magnetization axis was normalized by assuming equal values for the two curves at the single point $T/T_C = 0.656$. The result is given in Fig. 2, where it is seen that, to within experimental accuracy, the functional relationship of Eq. (3) is unaffected by pressure.

However, as noted above, Eq. (3) is usually applied to a ferromagnet, whereas in the region of spontaneous moment van Laar has shown that Cr_5S_6 exhibits the Néel-type ferrimagnetic spin configuration shown in Fig. 3. The magnetic moments of the sublattices of the unit cell are then given by $\sum_\nu \vec{\sigma}_\nu$, where the subscript ν refers to the cation sites in Fig. 3. Therefore our results as given in Fig. 2 establish only that $\sum_\nu \vec{\sigma}_\nu$ obeys Eq. (3) with $f(T/T_C)$ independent of pressure, rather than the more stringent requirement that this be true for each of the sublattice moments independently. However, it would be remarkably fortuitous for the individual $f_\nu(T/T_C)$ to change in such a way that their sum remained constant throughout the entire ferrimagnetic temperature interval. Hence our results strongly

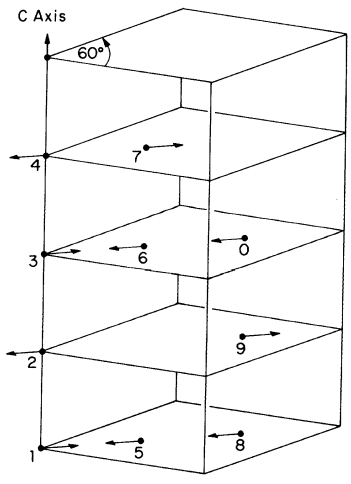

FIG. 3. Unit cell of Cr_5S_6, showing the ten different cation sites with the subscripts used in this paper to identify them, and showing the collinear ferrimagnetic spin configuration found above the transition temperature.

suggest that pressure does cause a significant change in the intrinsic moment of the chromium in Cr_5S_6.

This variation of moment with pressure and van Laar's[6] results, which showed approximately equal and nonintegral moments at the various chromium sites instead of the distinct integral values expected for an ordered array of Cr^{2+} and Cr^{3+} ions, are not phenomena normally associated with localized models. Although variation in spin-orbit mixing of nearly degenerate up- and down-spin levels might account satisfactorily for these phenomena within such a model, a collective-electron explanation in terms of slight shifts between nearly degenerate up- and down-spin bands would appear more natural. In addition, the presence of itinerant electrons is suggested by the observation of metallic conductivity in Cr_5S_6.[13]

III. MAGNETIC INTERACTIONS

In his neutron-diffraction study of Cr_5S_6, van Laar[6] used molecular field considerations to compare the relative energies of the observed antiferromagnetic and ferrimagnetic spin configurations as functions of the magnetic interaction energies. However, there was no attempt to establish the stability of these configurations relative to others, and the assumed signs of some of the magnetic interactions were highly questionable. It therefore appeared worthwhile to undertake a more complete study of the classical ground state in Cr_5S_6, where the classical ground state is defined as that spin arrangement which minimizes the Heisenberg exchange energy. Although there is some question regarding the validity of the Heisenberg Hamiltonian as applied to a high-conductivity material, it has proved a fruitful approach in other such materials and it is of interest to establish its ability to account for the observed magnetic properties of Cr_5S_6. The classical Heisenberg energy is given by

$$E=\sum' \bar{J}_{n\nu,m\mu}\,\vec{S}_{n\nu}\cdot\vec{S}_{m\mu}\,, \tag{4}$$

where $\vec{S}_{n\nu}$ and $\vec{S}_{m\mu}$ are unit vectors along the direction of spin quantization, n and m run over the unit cells of the sample, ν and μ run over the ten different sites within a unit cell shown in Fig. 3, and the $\bar{J}_{n\nu,m\mu}$ are the exchange constants multiplied by the spin magnitudes.

There are nine distinct nearest-neighbor (nn) interactions to be considered. They can be defined in terms of $\bar{J}_{\nu\mu}$, noting that, in general, $\bar{J}_{\nu\mu}=\bar{J}_{\mu\nu}$. Two of the interactions occur along the c axis. They are defined as

$$\bar{J}_1\equiv\bar{J}_{12}=\bar{J}_{23}=\bar{J}_{34}=\bar{J}_{14},\quad (C_{ab}) \tag{5a}$$

$$\bar{J}_{1'}\equiv\bar{J}_{57}=\bar{J}_{67}=\bar{J}_{89}=\bar{J}_{90}\,,\quad (C_{cf'}) \tag{5b}$$

where the subscript 0 refers to $\nu=10$. There are three distinct interactions in the a plane, defined by

$$\bar{J}_2\equiv\bar{J}_{15}=\bar{J}_{36}=\bar{J}_{30}=\bar{J}_{18}\,,\quad (C_{bf}) \tag{5c}$$

$$\bar{J}_{2'}\equiv\bar{J}_{47}=\bar{J}_{29},\quad (C_{ac}) \tag{5d}$$

$$\bar{J}_{2''}=\bar{J}_{58}=\bar{J}_{60},\quad (C_{ff}) \tag{5e}$$

and there are four distinct interactions with diagonal linkages, namely,

$$\bar{J}_3\equiv\bar{J}_{17}=\bar{J}_{37}=\bar{J}_{19}=\bar{J}_{39}\,,\quad (C_{bc}) \tag{5f}$$

$$\bar{J}_{3'}\equiv\bar{J}_{25}=\bar{J}_{26}=\bar{J}_{48}=\bar{J}_{40}\,,\quad (C_{af}) \tag{5g}$$

$$\bar{J}_{3''}\equiv\bar{J}_{28}=\bar{J}_{20}=\bar{J}_{45}=\bar{J}_{46}\,,\quad (C_{af'}) \tag{5h}$$

$$\bar{J}_{3'''}\equiv\bar{J}_{59}=\bar{J}_{69}=\bar{J}_{78}=\bar{J}_{70}\,,\quad (C_{cf}) \tag{5i}$$

where the van Laar symbol for the respective interactions are given in parentheses. Although our initial considerations will be limited to the nn interactions listed above, it will be shown that a spiral configuration requires the presence of next-nearest-neighbor (nnn) interactions as well. We will restrict ourselves to the set of such interactions along the c axis. They are defined by

$$\bar{J}_4\equiv\bar{J}_{13}\,, \tag{5j}$$

$$\bar{J}_{4'}\equiv\bar{J}_{24}\,, \tag{5k}$$

$$\bar{J}_{4''}\equiv\bar{J}_{56}=\bar{J}_{80}\,,\ \text{(with intervening cation present)} \tag{5l}$$

$$J_{4'''}\equiv J_{56}=J_{80}\,,\ \text{(with intervening vacancy).} \tag{5m}$$

IV. GROUND-STATE CALCULATION

In order to study the ground-state energy problem in Cr_5S_6, which has nonequivalent spins on the various sites, it is necessary to use the generalized Luttinger-Tisza (GLT) method.[7] In this method, the minimization of the energy of Eq. (4) reduces to the problem of finding the lowest eigenvalue of an interaction matrix function $\underline{\mathcal{L}}(\vec{k})$, where the propagation vector $\vec{k}$ varies over the first Brillouin zone, and the resulting spin configuration is directly related to the associated eigenvector. The mathematical details are discussed in Appendixes A and B.

The GLT method is particularly powerful in trying to establish the ground state of a coplanar spiral, such as was observed in Cr_5S_6, because of the theorem which states that, whenever a coplanar configuration is locally stable, the GLT method works and proves it to be the ground state; and that, whenever the GLT method fails for a coplanar configuration, it is unstable and cannot be the ground state.[14] The spiral configuration of Cr_5S_6, as determined by van Laar,[6] is shown in Fig. 4.

Our initial consideration were limited to the case of nn interactions only; that is, the interactions of the J_4 set [Eqs. (5j)–(5m)] were taken as zero. For this case it was found that, while the configurations varied considerably as functions of the interaction parameters, the resultant configuration always corresponded to a $\vec{k}=0$ mode. A spiral con-

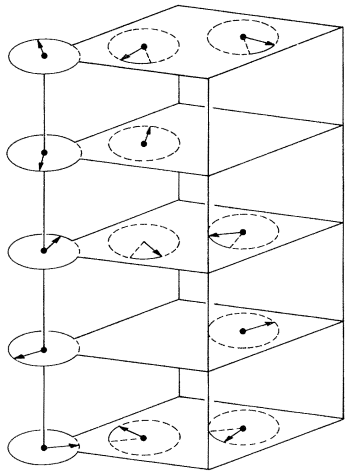

FIG. 4. Spiral spin configuration observed by van Laar in Cr_5S_6 at liquid-helium temperature.

figuration was never obtained as the ground state.

Apparently, it is always possible to minimize the energy within the $\vec{k}=0$ mode by a suitable canting of the spins. A map showing the different ground-state regions for a particular set of interaction relationships is given in Fig. 5; in it the boundaries between the different types of configurations arise either from the onset of canting or from

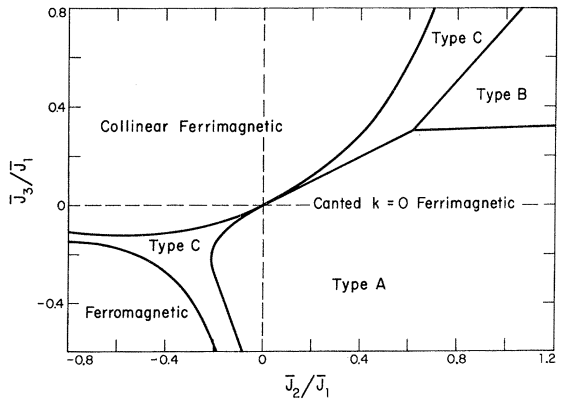

FIG. 5. Ground spin-state regions for the Cr_5S_6 lattice with $\bar{J}_1' = \bar{J}_1$, $\bar{J}_2' = \bar{J}_2 = \bar{J}_2$, $\bar{J}_3''' = \bar{J}_3'' = \bar{J}_3' = \bar{J}_3$, and no distant-neighbor interactions. The collinear ferrimagnetic configuration consists of ferromagnetic c planes arranged antiferromagnetically along the c axis. In the canted $\vec{k}=0$ configuration, $\vec{S}_4$ cants opposite to $\vec{S}_2$, $\vec{S}_9$ opposite $\vec{S}_7$, and $\vec{S}_8$ and $\vec{S}_{10}$ opposite to $\vec{S}_5$ and $\vec{S}_6$, with three distinct angles. The existence of internal boundaries within its ground-state region suggests that the canted configuration be subdivided into three types (A, B, and C) according to whether the near-neighbor correlation within c planes is essentially antiferromagnetic (A and B) or ferromagnetic (C) and whether that along the c axis is essentially antiferromagnetic (A and C) or ferromagnetic (B).

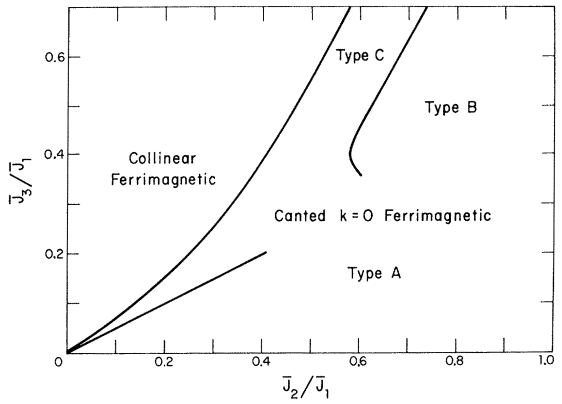

FIG. 6. Ground spin-state regions for $2\bar{J}_1' = \bar{J}_1$, $\bar{J}_2''' = \bar{J}_2' = \bar{J}_2$, $3\bar{J}_3''' = 6\bar{J}_3'' = 3\bar{J}_3' = 5\bar{J}_3$, and no distant-neighbor interactions. Although the clear-cut subdivision of the canted spin configuration into distinct types is eliminated by differentiation within the $\bar{J}_1$ and $\bar{J}_3$ families of interactions, there is no significant change in the boundaries between different $\vec{k}=0$ ground states.

discontinuities in the canting angles. Differentiation among the vertical, horizontal, or diagonal interactions does not qualitatively alter the topology of this map – it merely serves to weaken the discontinuities, as illustrated by a comparison of Fig. 6 with Fig. 5. The meaning of the boundaries of Fig. 6 is presented in Fig. 7, where one of the canting angles is plotted as a function of the interaction parameters.

Because of the great flexibility of the canted $\vec{k}=0$ modes, nnn interactions must be introduced in order to obtain a spiral configuration. Since the spins of c-axis nn neighbors are paired in the $\vec{k}=0$ eigenvectors, interactions between such pairs should

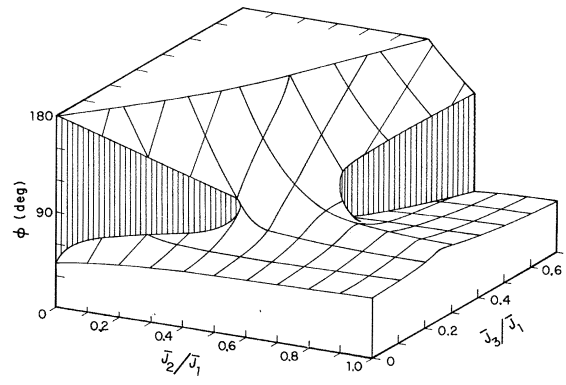

FIG. 7. The phase angle ϕ associated with $\vec{S}_5$, $\vec{S}_6$, $\vec{S}_8$, and $\vec{S}_0$ shown as a function of $\bar{J}_2/\bar{J}_1$ and $\bar{J}_3/\bar{J}_1$ for the same interactions as in Fig. 6. The discontinuities in ϕ illustrate the meaning of the boundaries plotted in Fig. 6.

be most effective in inducing spirals. For this reason, the limited set of nnn interactions specified by Eqs. (5j)–(5m) were chosen, where all the interactions are along the c axis. Although there is no *a priori* reason for expecting other nnn interactions to be smaller than those considered, they should be less effective, and all should be small compared to $\bar{J}_1$.

The introduction of small $\bar{J}_4$ interactions has a profound effect on the ground-state spin configurations. The value $\bar{J}_{4'''} = 0.01\bar{J}_1$ suffices to destabilize the $\vec{k}=0$ mode in the vicinity of the boundary shown in Fig. 5 at $\bar{J}_3 = 0.33\bar{J}_1$, $\bar{J}_2 > 0.6\bar{J}_1$. However the resulting configuration is a linear combination of $\vec{k}=0$ and $\vec{k}\neq 0$ modes, and hence presumably is of the conical type. Somewhat larger values of the nnn interactions are required before a pure spiral of the type described by van Laar[6] becomes the ground state for any set of nn interactions.

A map of the ground-state regions for $\bar{J}_4 = \bar{J}_{4'} = \bar{J}_{4''} = \bar{J}_{4'''} = 0.05\bar{J}_1$ is presented in Fig. 8 for the same set of nn interactions as were mapped in Fig. 5, so that a comparison of these two figures gives a dramatic demonstration of the effects of small nnn interactions. The ground-state region for the type of spiral observed in Cr_5S_6 is restricted to small values of $\bar{J}_3/\bar{J}_1$; the region labeled $\vec{k}<0$ in Fig. 8 involves the opposite sign for the phase angle. These ground-state regions are bounded for the most part by a conical spiral – only for negative $\bar{J}_3/\bar{J}_1$ can one pass directly from a van Laar spiral to a $\vec{k}=0$ ground state.

Although the boundaries of the ground-state region of the Cr_5S_6-type spiral shift somewhat as the nn interactions are varied, its general shape and location remain as depicted in Fig. 8. Consequently, it appears that the $\bar{J}_3$ family of interactions in Cr_5S_6 are probably antiferromagnetic ($\bar{J}_3/\bar{J}_1 > 0$) and relatively weak ($\bar{J}_3 < \bar{J}_2 < \bar{J}_1$), contrary to van Laar's assumption. However, the length of the spiral propagation vector $\vec{k}_0$ is so sensitive to differentiation within the $\bar{J}_3$ and $\bar{J}_4$ families that comparison of van Laar's results with our ground-state calculations yields rather mild restrictions upon the permissible ranges of interaction strengths. For this reason, we shall turn to the thermal evolution of the spiral ground state for further information.

V. CONFIGURATION AT FINITE TEMPERATURE

Following the treatment of Lyons *et al.*,[14] it can be shown in the quantum-mechanical molecular field approximation that $kT_C = -\frac{2}{3}\bar{J}_1\lambda_C$, where λ_c is the minimum eigenvector of the matrix function $\underline{\mathcal{L}}(\vec{k})$ defined by setting $\beta_\nu = [(S_\nu+1)/S_\nu]^{1/2}$, where S_ν is the spin quantum number for the νth site. Then the eigenvector associated with λ_C yields the spin configuration appropriate to T_C. Given values for the exchange interactions such that the Cr_5S_6-type spiral

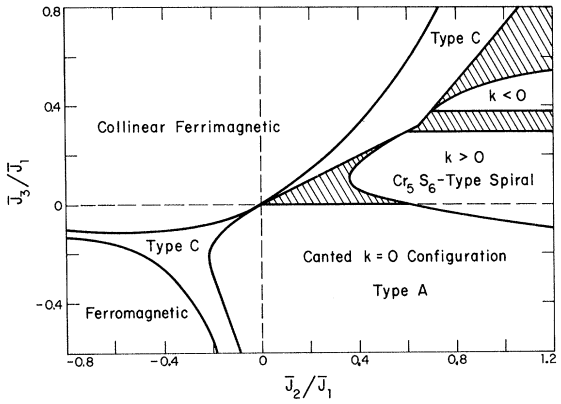

FIG. 8. Ground spin-state regions for the Cr_5S_6 lattice with $\bar{J}_{1'} = \bar{J}_1$, $\bar{J}_{2''} = \bar{J}_{2'} = \bar{J}_2$, $\bar{J}_{3'''} = \bar{J}_{3''} = \bar{J}_{3'} = \bar{J}_3$, and $\bar{J}_{4'''} = \bar{J}_{4''} = \bar{J}_{4'} = \bar{J}_4 = 0.05\bar{J}_1$. Comparison with Fig. 5 shows the effect of the distant-neighbor interactions. The ground-state spin configuration within the shaded regions are conical spirals with both $\vec{k}=0$ and $\vec{k}\neq 0$ Fourier components.

is the ground state, this high-temperature minimum eigenvector arises from the 4×4 submatrix of $\underline{\mathcal{L}}(0)$ and agrees with the ferrimagnetic alignment observed by van Laar,[6] provided the nnn interactions are not too strong. This result shows that a transition from an antiferromagnetic spiral at low temperatures to a collinear ferrimagnetic configuration at higher temperatures can be obtained within the molecular field approximation.

In this approximation, the magnetic free energy for Cr_5S_6 can be written as

$$\frac{F_M}{\bar{J}_1} \equiv \sum_{n\nu}\left\{\langle\vec{S}_{n\nu}\rangle\cdot\vec{H}'_{n\nu} - \frac{kT}{\bar{J}_1}\ln\left[\sinh\left(\frac{(2S_\nu+1)H'_{n\nu}\bar{J}_1}{kTS_\nu}\right)\right] + \frac{kT}{\bar{J}_1}\ln\left[\sinh\left(\frac{H'_{n\nu}\bar{J}_1}{kTS_\nu}\right)\right]\right\}, \tag{6}$$

where $\langle\vec{S}_{n\nu}\rangle$ is the thermal average of the spin vector $\vec{S}_{n\nu}$ and[15]

$$\vec{H}'_{n\nu} = -\sum_{m\mu}\frac{\bar{J}_{n\nu,m\mu}}{\bar{J}_1}\langle\vec{S}_{m\mu}\rangle.$$

We have written a FORTRAN computer program which uses a combination of the simplex[16] and Newton-Raphson methods to minimize this expression with respect to the length of the spin propagation vector, the Cr_5S_6-type phase angle, and the average length of the spin vectors at the four distinct types of lattice sites. Some of our results are presented in Fig. 9, where the thermal variations of the propagation vector $\vec{k} = (2\pi/c_0)(0,0,l)$ and of the net magnetization are compared with experiment on a normalized temperature scale. The thermal variation of the phase angle is not shown because of its similarity to that of $\vec{k}$.

The solid curves were computed for

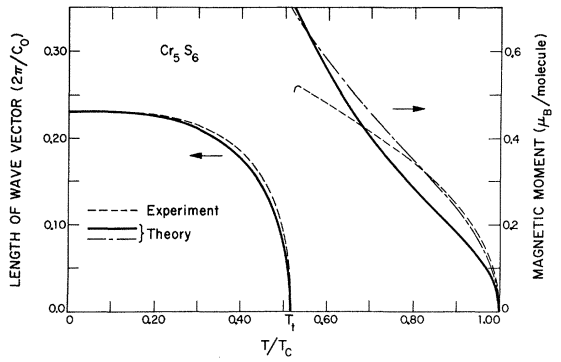

FIG. 9. Comparison between the observed thermal variations of the spiral propagation vector and ferrimagnetic moment of Cr_5S_6 with the results of our molecular field free-energy minimization. The two calculated magnetization curves illustrate the dependence of their shape upon the assumed set of interaction ratios. The values of these ratios used in the calculations are given in the text.

$$\bar{J}_{1'}=0.7\bar{J}_1,\quad \bar{J}_2=\bar{J}_{2'}=0.5\bar{J}_1,$$
$$\bar{J}_{2''}=0.85\bar{J}_2,\quad \bar{J}_3=\bar{J}_{3'}=\bar{J}_{3''}=\bar{J}_{3'''}=0.1\bar{J}_1,$$
$$\bar{J}_4=\bar{J}_{4'}=\bar{J}_{4''}=\bar{J}_{4'''}=0.05\bar{J}_1,$$

which yield the Cr_5S_6-type spiral for the ground state. The dashed curve below the transition point reproduces the thermal variation of the spiral propagation vector observed by van Laar. Comparison with the solid curve shows that our molecular field calculation gives reasonably good agreement with experiment from absolute zero up to the transition. However, it should be pointed out that the shape of the $\vec{k}$-versus-T curve is rather insensitive to those variations in interaction strengths which leave T_t and $\vec{k}(T=0\,^\circ\mathrm{K})$ invariant.

Above T_t, the dashed curve in Fig. 9 reproduces our present measurements of σ versus T in an applied field of 8 kOe. Although qualitatively similar, the solid curve does not give good quantitative agreement. Somewhat better agreement can be obtained with different values for the interactions, such as

$$\bar{J}_{1'}=0.5\bar{J}_1,\quad \bar{J}_2=\bar{J}_{2'}=\bar{J}_{2''}=0.5\bar{J}_1,$$
$$\bar{J}_3=\bar{J}_{3'}=\bar{J}_{3''}=\bar{J}_{3'''}=0,\quad \bar{J}_{4''}=0,$$
$$\bar{J}_4=\bar{J}_{4'}=\bar{J}_{4'''}=0.05\bar{J}_1,$$

as shown by the interrupted curve in Fig. 9. However, since the calculated net magnetization of 0.6 μ_B/molecule represents the difference between 5.44 and 4.84 μ_B, it is very sensitive to the values chosen for $g_\nu S_\nu$. We assumed that $S_\nu=\frac{3}{2}$ for all ν and adjusted g_ν to agree with the sublattice moment determined by van Laar at 4.2 °K, but these values are not sufficiently well known to warrant a serious attempt to optimize the fit to the magnetization data. Knowledge of the sublattice moments at 208 °K ($0.7T_C$) would provide a useful check, but the values reported by van Laar are not compatible with the observed magnetization. In any case, the existence of good qualitative agreement between experiment and our molecular field calculation is of much greater significance, within the context of this paper, than any question of detailed quantitative fit.

VI. CONCLUSIONS

Using a Heisenberg model, we have shown that the observed spiral ground-state spin configuration in Cr_5S_6 requires not only that all of the nn exchange interactions be antiferromagnetic, but also that antiferromagnetic nnn interactions be present. Furthermore, taking a set of interactions consistent with the observed ground state, we have shown that a molecular field calculation yields good agreement with the observed thermal variation of the spiral configuration and predicts a second-order spin transition to the observed high-temperature ferrimagnetic configuration. Thus the transition arises from a shift in the relative effectiveness of the various interactions because of the different temperature dependencies of the average spins on the different sublattices. This is, to our knowledge, the first example of an antiferromagnetic-ferrimagnetic transition in which the primary mechanism for the transition arises from the thermal variation of the moments within the molecular field approximation without requiring a variation in the exchange interaction values, in contrast to the exchange inversion model introduced by Kittel, which was based upon the exchange interaction being a linear function of a lattice parameter and crossing zero at some critical value of this parameter.[17]

We conclude that the transition in Cr_5S_6 is fundamentally of second order, as indicated experimentally by the continuous variation of the spiral propagation vector and by the gradualness of the transition. Admittedly, the observation of thermal hysteresis requires the existence of metastable states, but experiment shows that the passage between these states is continuous, and does not involve the sudden jump found in first-order transitions. We propose the mechanism for this continuous passage to be a conical (ferrimagnetic) spiral spin configuration. Such a modification of an antiferromagnetic spiral configuration is to be expected in the presence of an applied magnetic field. Furthermore, the field dependence of its cone angles would result in a field-dependent shape for the transition curve, in agreement with the behavior observed when cooling through the transition in Cr_5S_6. During cooling, anisotropy and magnetostrictive forces could combine with the applied field to hold the net magnetization in the easy c plane,[6] which would force a spiral spin component out of this plane

and would thereby lower the transition temperature. In the antiferromagnetic state, however, there is no net moment in the easy plane[6] and probably too small a perpendicular susceptibility to cause a spin flip, so that the warming transition might not occur until $\vec{k}$ became very small. This model seems plausible and appears to account for the observed phenomena.

Despite the success of the Heisenberg model in accounting for the observed magnetic behavior of Cr_5S_6, it appears almost certain that some of its magnetism must result from band phenomena. The strongest evidence for this conclusion consists of our observation of a significant pressure dependence of σ_0 and van Laar's observation of almost equal nonintegral moments on all the sublattices at 4.2 °K instead of unequal integral ionic values, which are both difficult to explain on a localized basis. Further confirmation comes from our observation of a large negative value for $(\partial T_C/\partial P)$, which implies a decrease in some of the interactions since we show them all to be antiferromagnetic. Localized models predict that antiferromagnetic interactions must increase with decreasing ionic separation, whereas a simple band model can lead to a decreasing interaction with decreasing ionic separation, because of increasing bandwidth.[18] For the case of Cr_5S_6, where we conclude both localized and collective electrons are contributing to the magnetic interactions, it is impossible to predict the net effect without detailed information regarding the nature and the magnitude of the various interactions.

Because of the large decrease of T_C with pressure (nearly 1% per kbar), the very small increase of T_t with pressure represents a moderate increase of the ratio T_t/T_C. This effect can most easily be attributed to an increase in the nnn interactions relative to $\bar{J}_1$. In additon, we find the shape of the normalized magnetization-versus-temperature curve to be independent of pressure. Since this shape is sensitive to variations among the other interactions, we can conclude that the primary effect of pressure is to decrease the value of $\bar{J}_1$. This conclusion is consistent with the fact that $\bar{J}_1$ represents the interaction across the smallest intercation spacing in Cr_5S_6, and hence is the most likely to involve electron-band behavior.

APPENDIX A: APPLICATION OF GLT METHOD

In the GLT method,[7] the Heisenberg energy of Eq. (4) is minimized subject to the "weak" constraint that

$$\sum_{n\nu} \beta_\nu^{-2} \vec{S}_{n\nu} \cdot \vec{S}_{n\nu} = N \sum_\nu \beta_\nu^{-2} \ , \tag{A1}$$

where the parameters β_ν are initially arbitrary but are uniquely determined in the process of applying the method. The resulting minimum energy is given by

$$\mathcal{E} = E/(N\bar{J}_1) = \lambda_0 \textstyle\sum_\nu \beta_\nu^{-2} \ , \tag{A2}$$

where λ_0 is the minimum eigenvalue – minimum over all branches and all wave vectors $\vec{k}$ – of the matrix function

$$\mathfrak{L}_{\nu\mu}(\vec{k}) = \beta_\nu \beta_\mu \textstyle\sum_m (\bar{J}_{n\nu, m\mu}/\bar{J}_1) \exp[i\vec{k} \cdot (\vec{R}_{m\mu} - \vec{R}_{n\nu})] \ , \tag{A3}$$

where $(\vec{R}_{m\mu} - \vec{R}_{n\nu})$ is the vector separation of the interacting sites. It is often possible to choose the β_ν so that a physical spin configuration (comprised of unit spin vectors) can be constructed from some linear combination of degenerate eigenvectors associated with the minimum eigenvalue λ_0. Whenever this occurs, the GLT reasoning proves the resulting configuration to be the ground state.[7]

As shown in Fig. 3, the unit cell of Cr_5S_6 contains ten cations. However, these occupy just four crystallographically distinct types of sites.[1,6] This circumstance reduces the number of independent β_ν to four, so that we define

$$\beta_5 = \beta_6 = \beta_8 = \beta_{10} = 1, \quad \beta_1 = \beta_3 = \beta_b,$$

$$\beta_2 = \beta_4 = \beta_a, \quad \beta_7 = \beta_9 = \beta_c \ .$$

The resulting matrix $\underline{\mathfrak{L}}(\vec{k})$ is given in Appendix B for $\vec{k}$ along the hexagonal axis.

When $\vec{k} = 0$, this matrix factors into 4×4, 1×1, 3×3, and 2×2 submatrices. The eigenvectors of the 4×4 have the form $\underline{\Psi} = (\Psi_1, \Psi_2, \ldots, \Psi_{10}) = (b, a, b, a, f, f, c, f, c, f)$, while the 3×3 gives $(0, a', 0, -a', f', f', c', -f', -c', -f')$. The collinear spin configurations of Figs. 5–8 were constructed from the eigenvector associated with the minimum eigenvalue λ_0 of the 4×4 submatrix by requiring that

$$\beta_a^2 a^2 = \beta_b^2 b^2 = \beta_c^2 c^2 = f^2 .$$

This determination of the parameters β_ν specifies a particular matrix function $\underline{\mathfrak{L}}(\vec{k})$, and by numerical evaluation using an IBM dual 360/67 computer we found λ_0 to be the minimum eigenvalue of this particular $\underline{\mathfrak{L}}(\vec{k})$ for *all* values of $\vec{k}$ in the first Brillouin zone within the regions indicated as collinear in Figs. 5–8.

An eigenvalue of the 3×3 submatrix becomes degenerate with λ_0 along the boundaries of the collinear regions. Beyond these boundaries it is necessary to adjust β_b to maintain this degeneracy. Consequently, one is led to the canted configurations of Figs. 5–8, where the 4×4 eigenvector is assigned to one component of the spins and the 3×3 eigenvector to another. Then β_a, β_c and the coefficient of linear combination of the two eigenvectors can be evaluated to yield unit spin vectors. This procedure again determines a particular function $\underline{\mathfrak{L}}(\vec{k})$, for which λ_0 was found to be the minimum eigenvalue over *all* $\vec{k}$ in the first Brillouin zone throughout the regions of canted configurations shown in Figs. 5–8.

Boundaries between different canted regions arise from transitions to a different eigenvector branch, which results in a discontinuity in at least one of the canting angles, as shown in Fig. 7.

When the nnn interactions become sufficiently strong, there appears another boundary along which some eigenvalue $\lambda_1(\vec{k}_0)$ for finite $\vec{k}_0$ along the hexagonal axis becomes degenerate with λ_0. Beyond this boundary, the ground state must involve the eigenvector associated with $\lambda_1(\vec{k}_0)$, which has the form $(b, a, b, a, f+if', f-if', c, f-if', c, f+if')$. If the β_ν are adjusted so as to yield unit spin vectors just from this eigenvector and its conjugate, the van Laar-type spiral is obtained and a particular $\underline{\mathcal{L}}(\vec{k})$ is determined. As seen in Fig. 8, there is a region where $\lambda_1(\vec{k}_0)$ is the minimum eigenvalue of this $\underline{\mathcal{L}}(\vec{k})$ for *all* $\vec{k}$ when

$$\bar{J}_4 = \bar{J}_{4'} = \bar{J}_{4''} = \bar{J}_{4'''} = 0.05\,\bar{J}_1 .$$

Along the boundary of this region, an eigenvalue of $\underline{\mathcal{L}}(0)$ becomes degenerate with $\lambda_1(\vec{k}_0)$. However, in general, this boundary does not coincide with the $\lambda_1(\vec{k}_0) = \lambda_0$ boundary of the canted $\vec{k} = 0$ mode because the relationships determining β_ν, and hence the functions $\underline{\mathcal{L}}(\vec{k})$ themselves, are different in the two regions. The ground state in the space between these two boundaries must be associated with a linear combination of eigenvectors for $\vec{k} = +\vec{k}_0$ and $\vec{k} = 0$, and such a linear combination yields a conical spiral.

APPENDIX B: MATRIX $\underline{\mathcal{L}}(\vec{k})$

When $\vec{k}$ is along the c axis, we can write $\vec{k} = (2\pi/c_0) \times (0, 0, l)$. Then, defining

$$\zeta = \cos\tfrac{1}{2}\pi l + i \sin\tfrac{1}{2}\pi l \ ,$$

$$\eta = \cos\pi l + i \sin\pi l \ ,$$

we have for $\mathcal{L}_{\nu\mu}$ (writing $\mu = 0$ for $\mu = 10$)

$$\mathcal{L}_{12} = \mathcal{L}_{23} = \mathcal{L}_{34} = \mathcal{L}_{14}^* = \beta_1\beta_2\zeta \ ,$$

$$\mathcal{L}_{67} = \mathcal{L}_{89} = \mathcal{L}_{90} = \mathcal{L}_{57}^* = \beta_3\zeta\bar{J}_2/\bar{J}_1 \ ,$$

$$\mathcal{L}_{15} = \mathcal{L}_{18} = \mathcal{L}_{36} = \mathcal{L}_{30} = 3\beta_1\bar{J}_3/\bar{J}_1 \ ,$$

$$\mathcal{L}_{28} = \mathcal{L}_{47} = 3\beta_2\beta_3\bar{J}_4/\bar{J}_1 \ ,$$

$$\mathcal{L}_{58} = \mathcal{L}_{69} = 3\bar{J}_5/\bar{J}_1 \ ,$$

$$\mathcal{L}_{19} = \mathcal{L}_{17} = \mathcal{L}_{37} = \mathcal{L}_{39}^* = 3\beta_1\beta_3\zeta\bar{J}_6/\bar{J}_1 \ ,$$

$$\mathcal{L}_{26} = \mathcal{L}_{25}^* = \mathcal{L}_{48} = \mathcal{L}_{40}^* = 3\beta_2\zeta\bar{J}_7/\bar{J}_1 \ ,$$

$$\mathcal{L}_{20} = \mathcal{L}_{28}^* = \mathcal{L}_{45} = \mathcal{L}_{46}^* = 3\beta_2\zeta\bar{J}_8/\bar{J}_1 \ ,$$

$$\mathcal{L}_{59} = \mathcal{L}_{69}^* = \mathcal{L}_{78}^* = \mathcal{L}_{70} = 3\beta_3\zeta\bar{J}_9/\bar{J}_1 \ ,$$

$$\mathcal{L}_{56} = \mathcal{L}_{80}^* = \eta\bar{J}_{10}/\bar{J}_1 + \eta^*\bar{J}_{11}/\bar{J}_1 \ ,$$

$$\mathcal{L}_{13} = \beta_1^2(\eta + \eta^*)\bar{J}_{12}/\bar{J}_1 \ ,$$

$$\mathcal{L}_{24} = \beta_2^2(\eta + \eta^*)\bar{J}_{12}/\bar{J}_1 \ ,$$

$$\mathcal{L}_{35} = \mathcal{L}_{68} = \mathcal{L}_{79} = \mathcal{L}_{\nu\nu} = \mathcal{L}_{\nu\nu+5} = 0 \ ,$$

$$\mathcal{L}_{\mu\nu} = \mathcal{L}_{\nu\mu}^* \ .$$

---

†Work sponsored by the Department of the Air Force.

[1]F. Jellinek, Acta Cryst. 10, 620 (1957).

[2]T. Kamigaichi, K. Masumoto, and T. Hihara, J. Phys. Soc. Japan 15, 1355 (1960).

[3]H. Haraldsen and A. Neuber, Z. Anorg. Allgem. Chem. 234, 337 (1937); 234, 372 (1937).

[4]M. Yuzuri, T. Hirone, H. Watanabe, S. Nagasaki, and S. Madea, J. Phys. Soc. Japan 12, 385 (1957).

[5]K. Dwight, R. W. Germann, N. Menyuk, and A. Wold, J. Appl. Phys. 33, 1341 (1962).

[6]B. van Laar, Phys. Rev. 156, 654 (1967).

[7]D. H. Lyons and T. A. Kaplan, Phys. Rev. 120, 1580 (1960).

[8]T. Kamigaichi, T. Okamoto, N. Iwata, and E. Tatsumoto, J. Phys. Soc. Japan 21, 2730 (1966).

[9]N. Menyuk, J. A. Kafalas, K. Dwight, and J. B. Goodenough, Phys. Rev. 177, 942 (1969).

[10]R. B. Flippen and F. J. Darnell, J. Appl. Phys. 34, 1094 (1963).

[11]In order to check on the effect of composition, we also measured the effect of pressure on the transition temperature of a sample of $CrS_{1.17}$. We obtained the value $\partial T_t/\partial P = -0.34$ deg/kbar, which also disagrees significantly with the results of Ref. 8. It is impossible to establish the cause of this difference. It may lie in sample disparities because of different methods of preparation or, alternatively, the electrical conductivity kink may not be as well correlated with T_t as was assumed on the basis of measurements at atmospheric pressure.

[12]J. S. Kouvel, in *Solids under Pressure*, edited by W. Paul and D. M. Warschauer (McGraw-Hill, New York, 1963), Chap. 10, p. 284.

[13]C. F. van Bruggen and F. Jellinek, Colloque International sur les dérivées semi-metallique du Centre National de la Recherche Scientifique, Orsay, 1965, p. 32 (unpublished).

[14]D. H. Lyons, T. A. Kaplan, K. Dwight, and N. Menyuk, Phys. Rev. 126, 540 (1962).

[15]N. Menyuk, K. Dwight, and A. Wold, J. Phys. (Paris) 25, 528 (1964).

[16]J. A. Nelden and R. Mead, Computer J. 7, 308 (1965).

[17]C. Kittel, Phys. Rev. 120, 335 (1960). In the Introduction, Kittel even commented that such transitions (ferro- or ferrimagnetic to antiferromagnetic) were not expected to occur, as far as he knew, within the framework of pure molecular field theory with temperature-independent interactions.

[18]J. B. Goodenough, Phys. Rev. 164, 785 (1967).